

IMPLICIT VECTORIAL OPERATOR SPLITTING FOR INCOMPRESSIBLE NAVIER — STOKES EQUATIONS IN PRIMITIVE VARIABLES*

(Paper dedicated to the memory of Professor N. N. Yanenko)

C. I. CHRISTOV

University of Louisiana at Lafayette, USA

e-mail: christov@louisiana.edu

R. S. MARINOVA

Free University of Varna, Bulgaria

Стационарные несжимаемые уравнения Навье — Стокса в исходных переменных дополняются уравнением Пуассона для давления, при этом уравнение неразрывности исключается и доказывается эквивалентность исходной задаче. Вводится “фиктивное” время и применяется расщепление векторных операторов так, что система остается связанной на каждом дробном шаге по “времени”, что позволяет выполнять граничные условия без введения искусственного условия для давления. Для конвективных членов применяются консервативные аппроксимации второго порядка на разнесенных сетках. В качестве примера рассматривается двумерное течение в прямоугольной каверне. В расчетах для чисел Рейнольдса до 11 000 и на сетках размерности 512×512 ячеек воспроизведено ламинарное течение. Результаты, полученные на различных сетках, подтверждают согласованность и сходимость схемы. Вычисленные характеристики течения для $Re \leq 10\,000$ качественно хорошо согласуются с известными численными решениями других авторов.

1. Introduction

The system of incompressible Navier — Stokes equations (N-S, for brevity) describes the motion of incompressible viscous liquid. The coupling of N-S system comes through the nonlinear terms, the continuity equation, and the boundary conditions.

In the numerical solution of the incompressible N-S, a serious difficulty arises from the determination of the pressure field. In fact, the continuity equation represents a constraint on the velocity field to be satisfied. At the time, the unknown pressure function provides the degree of freedom needed to accommodate such a constraint. Thus the pressure field is not calculated

*CIC acknowledges a summer research award from the University of Louisiana at Lafayette. The work of RSM was supported in part by Grant MM-610/96 from the National Science Foundation of Bulgaria. Permission to use the free software PSPLOT developed by Kevin E. Kohler from Nova Southeastern University is gratefully acknowledged.

© C. I. Christov, R. S. Marinova, 2001.

by an explicit time-advancement procedure but requires instead an implicit determination. This means that the incompressible N-S equations are not a system of Cauchy-Kovalevskaya type [42] and this aspect can be considered to be their most distinctive feature. Quite naturally, for the implicit pressure function no boundary conditions (b.c.) have to be prescribed at the rigid boundaries. This is still another formidable obstacle on the way of constructing fully implicit schemes. In 2D, the pressure can be eliminated from the equations by means of stream function ψ and vorticity function $\omega = -\nabla^2\psi$ ($\psi-\omega$ formulation) but then an explicit boundary condition for vorticity is missing.

The implicit nature of the pressure function (or the vorticity function) requires a special care for stability of algorithms since the explicit decoupling of the boundary conditions (descendant of the so-called Thom's condition) imposes significant limitations on the time increment ([30, 32, 38, 45, 11, 12, 26]) for stability. The literature abounds with different approaches to the problems of the iterative decoupling the system. The continuity equation is decoupled by means of Chorin's method of fractional steps (see [14, 27, 28, 1, 2]) in which the velocity field is predicted in the first half-time step and then the pressure is adjusted in the second half-time step so that the momentum equations are projected on approximately divergence-free vector field. A comprehensive account of the progress recently made along these lines can be found in [34, 24] where the 3D problem is also treated. This kind of methods are called semi-explicit.

In its turn, the problem with the boundary condition has also received considerable attention. In $\psi - \omega$ formulation the iterative Thom's condition was elaborated, e. g., in [18, 4]. Different algorithms for coupled solution of the $\psi - \omega$ equations were developed in [17, 35, 26] among many others. In primitive variables an algorithm for coupled solving Navier — Stokes equations with central differences in [46]. See, e. g., [20] for a comprehensive review on this subject.

The simplest and most obvious way of circumventing the difficulty caused by the lack of a boundary condition for the vorticity is not to use a vorticity function at all. In the so-called "stream function formulation", the simultaneous specification of the Dirichlet and Neumann boundary condition creates no difficulty, because the correct posing of the boundary value problem for the fourth-order elliptic operator ∇^4 involves two boundary conditions. To the limit of our knowledge, the first numerical solution of N-S with bi-harmonic equation for the stream function is attempted in [6]. The first implicit stream-function scheme is presented in [36]. One of the feasible ways to reduce the required computational time is to use a convergence method combined with operator splitting. This was a line followed in previous authors works where some of the specific problems connected with the fourth-order derivatives were corroborated. Following the idea of operator-splitting for bi-harmonic operators from [7] a fully implicit implementation of the boundary conditions is demonstrated in [11, 12] by means of an operator-splitting scheme for the fourth-order stream-function equation (see, also [9, 10] for some other applications of operator-splitting for bi-harmonic operators). A comprehensive account of this approach is due in an upcoming work [13].

Apart from the stream-function formulation, the implicit implementation of the boundary conditions in an operator-splitting method is still a problem, especially when N-S are kept in the form of a system of equations, e. g. primitive variables, or $\psi - \omega$ formulation. The only way to have implicit approximation when a system is considered is to use a vectorial splitting.

A vectorial operator splitting can be performed only for a system of evolution (Cauchy-Kovalevskaya type). Hence for the stationary $\psi - \omega$ system an artificial time can be added to each equation (called "false transients" in [30]). The operator splitting was used in [4] in the framework of the explicit Thom's condition. A vectorial version of the operator splitting which avoids using Thom's condition was developed for $\psi - \omega$ formulation as early as in [38] and a

specialized solver was created for the vectorial multidiagonal systems arising thereof.

The main purpose of the present paper is the implementation of vectorial splitting in primitive variables. If the Poisson equation for pressure is used instead of the continuity equation, one can add fictitious time and render the original system into an evolution system containing a set of three coupled parabolic equations for u, v and p . The primary difficulty with this approach is the specification of boundary conditions for pressure (see [20, 22, 24]). As pointed out in [24, 40], one-to-one correspondence to the original system holds if the continuity equation is satisfied on the boundaries while employing the normal component of the momentum equation cannot enforce the divergence to be equal zero and leads to an undermined system. This leads to an overposed problem for the velocity components if decoupled from the pressure. Another difficulty is connected with the so-called “compatibility condition” [20, 1, 2] for the pressure when decoupled from the momentum equations and subjected to Neumann b.c. Higher-order approximations, overlapping and composite grids are treated in [24, 25, 47].

In the present paper a vectorial version of the operator-splitting implicit scheme is proposed which preserves the coupling between the sought functions at each fractional time step allowing one to satisfy the boundary conditions without iterations. This circumvents altogether the problem with the *compatibility condition*. In the present work the approximation and stability of the scheme in full time steps is achieved after the continuity equation is added to the Poisson equation for the pressure and the resulting parabolic equation is dully split.

For the nonlinear terms we use an approximation with central differences which is *conservative* in the sense that it is free of artificial scheme viscosity and hence the approximation of the nonlinear terms does not affect the evolution of the total energy of the process.

We consider two-dimensional version of N-S equations only for the sake of simplicity. Unlike the stream-function and $\psi - \omega$ formulations, the proposed splitting method for primitive variables is readily extended to the 3D case.

In order not to obscure the main ideas of the method we consider in this paper only regions with rectilinear boundaries in cartesian coordinates. The grid is assumed uniform and staggered. The generalization to non-uniform grid distribution in each direction is trivial. As a featuring example is taken the lid-driven viscous incompressible flow in a square cavity. Driven cavity flow has always been a choice case study for each new scheme for N-S equations. The advantage of this test problem is that its geometry is the simplest possible. The disadvantage is that there are singularities in the points where the lid touches the vertical walls in the sense that the horizontal velocity component is double-valued there. It turns out, however, that the discontinuous boundary condition for horizontal velocity component does not pose real difficulties.

One of the important properties of the 2D lid-driven cavity flow is that the transition to turbulence appears to be delayed to very large Reynolds numbers. This makes it a very good testing ground for new schemes and algorithms. The abundant literature provides for the necessary checks for any new technique.

Regardless to its test nature the lid-driven cavity is hard enough to tackle numerically and its simulation is still a formidable task in the case of higher Reynolds numbers. The struggle for quantitatively precise prediction for high Reynolds numbers is still unfinished process in the literature. The second aim of the present paper is to provide accurate data for various flow characteristics.

2. Posing the Problem

Consider a closed 2D domain Ω with a piecewise smooth boundary $\partial\Omega$. The viscous incompressible flow in Ω is governed by the 2D Navier – Stokes equations

$$\frac{1}{\text{Re}} \left(\frac{\partial^2 u}{\partial x^2} + \frac{\partial^2 u}{\partial y^2} \right) - \frac{\partial p}{\partial x} - C[u] = 0, \quad (1)$$

$$\frac{1}{\text{Re}} \left(\frac{\partial^2 v}{\partial x^2} + \frac{\partial^2 v}{\partial y^2} \right) - \frac{\partial p}{\partial y} - C[v] = 0, \quad (2)$$

coupled by the continuity equation

$$\frac{\partial u}{\partial x} + \frac{\partial v}{\partial y} = 0. \quad (3)$$

Here (x, y) are the Cartesian coordinates, $u(x, y)$, $v(x, y)$ are the velocity components, and $p(x, y)$ is the pressure. The Reynolds number is defined as $\text{Re} = UL/\nu$, where U is the characteristic velocity, L – characteristic length, ν – kinematic coefficient of viscosity.

In the equations (1), (2) the operator $C = C_x + C_y$ is a short-hand notation for the advective terms. Using the incompressibility constraint (3) we can recast C_x and C_y in the form

$$C_x[f] = \frac{\partial u f}{\partial x} - \frac{f \partial u}{2 \partial x}, \quad C_y[f] = \frac{\partial v f}{\partial y} - \frac{f \partial v}{2 \partial y}, \quad (4)$$

where f stands for u or v , respectively.

It is readily shown that the operator C is skew-symmetric, namely that $(C[\varphi], \varphi) = 0$ for any φ from the considered space with trivial boundary conditions.

For internal flows with no free boundaries, the two velocity components are to be prescribed at the boundary $\partial\Omega$ (so-called no-slip conditions), namely

$$(u, v)|_{\partial\Omega} = (u_b, v_b). \quad (5)$$

If a portion of $\partial\Omega$ is a free boundary then the non-flux conditions for the velocity, say $\mathbf{v} \cdot \mathbf{n} = v_n$, together with the pressure distribution are to be specified. In a sense, such a case is simpler since one gets an explicit condition for each function at the boundary. In the case of internal flows (no free boundaries), the pressure p is an implicit function and no boundary conditions are available for it. In the present paper we focus our attention on the latter case.

Upon applying the operation div to (1), (2) and acknowledging the incompressibility constraint (3) one obtains an explicit relation for the pressure p called ‘‘Poisson equation for pressure’’

$$\frac{\partial^2 p}{\partial x^2} + \frac{\partial^2 p}{\partial y^2} + \frac{\partial C[u]}{\partial x} + \frac{\partial C[v]}{\partial y} = 0. \quad (6)$$

We multiply (6) by $1/\text{Re}$ and subtract from the result the continuity equation (3), namely

$$\frac{1}{\text{Re}} \left(\frac{\partial^2 p}{\partial x^2} + \frac{\partial^2 p}{\partial y^2} \right) - \frac{\partial u}{\partial x} - \frac{\partial v}{\partial y} + \frac{1}{\text{Re}} \left(\frac{\partial C[u]}{\partial x} + \frac{\partial C[v]}{\partial y} \right) = 0. \quad (7)$$

The advantages of (7) over (6) will be discussed in the section devoted on the operator splitting. The formulation with equation for pressure (7) is equivalent to the original system only if the continuity equation (3) is satisfied also on the boundary, namely

$$\left(\frac{\partial u}{\partial x} + \frac{\partial v}{\partial y} \right) \Big|_{(x,y) \in \partial\Omega} = 0. \quad (8)$$

Thus we arrive at a new boundary-value problem for the primitive variables u , v , and p . We prove the following

Theorem: Any solution of the system (1), (2), (7) subject to the boundary conditions (5), (8) is a solution of the original boundary value problem (1), (2), (3), and (5).

Proof: Take the sum of the x -derivative of (1) and y -derivative of (2) and from the result subtract (7) multiplied by Re . Then for the divergence $\delta \stackrel{\text{def}}{=} u_x + v_y$ we get the following boundary-value problem

$$\Delta\delta - \text{Re}^2\delta = 0 \quad \text{for} \quad (x, y) \in \Omega; \quad \delta = 0 \quad \text{for} \quad (x, y) \in \partial\Omega, \quad (9)$$

with (8) duly acknowledged. The boundary value problem (9) has a unique trivial solution, hence the continuity equation (3) is satisfied in the entire domain Ω .

The theorem provides the sufficient condition for one-to-one correspondence between the two formulations. The necessity follows directly from the way the new system is derived. Thus the equivalency between the two boundary value problems is established.

3. The Method of False Transients

The purpose of the present work is to construct an iterative algorithm for the steady-state flow. To this end in each equation of the governing system (1), (2), and (7) we add derivatives with respect to a fictitious time t rendering it into an evolution system, namely

$$\frac{\partial u}{\partial t} = \frac{1}{\text{Re}} \left(\frac{\partial^2 u}{\partial x^2} + \frac{\partial^2 u}{\partial y^2} \right) - \frac{\partial p}{\partial x} - C[u], \quad (10)$$

$$\frac{\partial v}{\partial t} = \frac{1}{\text{Re}} \left(\frac{\partial^2 v}{\partial x^2} + \frac{\partial^2 v}{\partial y^2} \right) - \frac{\partial p}{\partial y} - C[v], \quad (11)$$

$$\frac{\partial p}{\partial t} = \frac{1}{\text{Re}} \left(\frac{\partial^2 p}{\partial x^2} + \frac{\partial^2 p}{\partial y^2} \right) - \left(\frac{\partial u}{\partial x} + \frac{\partial v}{\partial y} \right) + \frac{1}{\text{Re}} \left(\frac{\partial C[u]}{\partial x} + \frac{\partial C[v]}{\partial y} \right). \quad (12)$$

Note, that the real physical non-stationary case requires retaining the physical time alongside with the artificial one (see, [12] for the stream-function formulation) and will be treated in a follow-up work.

The parabolic system (10), (11), and (12) can be considered as an extension to the case of primitive variables of what was called ‘‘Method of False Transients’’ in [30] for the $\psi - \omega$ formulation. After the convergence of the artificial-time process (the false transient) the steady solution is found. A different kind of false-transient algorithm was used in [39] where a time derivative of pressure was added to the continuity equation rendering thus the N-S system to an artificially compressible system of Cauchy-Kovalevskaya type.

We multiply (10) by u , (11) — by v , and (12) — by p . Then we integrate over the domain Ω and acknowledge the boundary conditions (5), (8). Since we are concerned with the stability of the above postulated evolution system (1), (2), (12) it suffices to consider only the trivial boundary conditions $u_b = 0, v_b = 0$. Upon acknowledging the boundary conditions we show that

$$\iint_{\Omega} \left(\frac{\partial pu}{\partial x} + \frac{\partial pv}{\partial y} \right) dx dy \equiv \oint_{\partial\Omega} pv_n ds = 0,$$

and get for the evolution of the total energy $\mathcal{E} \stackrel{\text{def}}{=} \iint_{\Omega} \frac{1}{2} [u^2 + v^2 + p^2] dx dy$, the following:

$$\frac{d\mathcal{E}}{dt} = - \iint_{\Omega} \frac{1}{\text{Re}} [(\nabla u)^2 + (\nabla v)^2 + (\nabla p)^2] dx dy + \iint_{\Omega} \frac{p}{\text{Re}} \left(\frac{\partial C[u]}{\partial x} + \frac{\partial C[v]}{\partial y} \right) dx dy. \quad (13)$$

Now, the importance of the term we added in the Poisson equation for pressure is clearly demonstrated. Without it, a non-definite term of unit order arises in the right hand side of equality (13). The effect of the term we added in the Poisson equation for pressure is to cancel the said term of unit-order which is not necessarily equal or close to zero in the initial stages of the iterative process. As a result the total energy evolves with a pace defined by the balance of two terms proportional to Re^{-1} the latter being a small number for the critical cases of small viscosity. In addition one of the terms is negative definite. All this means that the timewise changes of the total energy will be smooth enough (small time derivative proportional to Re^{-1}). The evolution of \mathcal{E} will come to an end when the rightmost term in (13) comes into a balance with the negative-definite one.

In its turn the divergent form of the nonlinear terms (4) secures that under the adopted boundary conditions, one gets for velocity components the following

$$\iint_{\Omega} \left(u \frac{\partial C[u]}{\partial x} + v \frac{\partial C[v]}{\partial y} \right) dx dy = \iint_{\Omega} \left(\frac{\partial u e^2}{\partial x} + \frac{\partial v e^2}{\partial y} \right) dx dy = \oint_{\partial\Omega} e^2 v_n ds = 0,$$

where $e^2 = \frac{1}{2}(u^2 + v^2)$ is the kinetic energy.

4. Vectorial Operator–Splitting

Having introduced the artificial time we render our system parabolic. Each iteration (artificial time step) is implemented via operator splitting. We choose the method of operator splitting because of its renown computational efficiency. In the present work we go further and use a vectorial splitting which enables us to avoid using explicit boundary conditions for the pressure. The rationale is that when the vectorial nature of the system for u , v , and p is preserved on each fractional time-step, then a boundary condition for the pressure is not necessary. The pressure at the boundary is defined by the overposed data for the velocity components stemming from the incompressibility constraint.

First we recast the equations for u , v and p into the following vectorial system

$$\frac{\partial \boldsymbol{\theta}}{\partial t} = (L_1 + L_2) \boldsymbol{\theta} + (C_1 + C_2) \boldsymbol{\theta} + \mathbf{F}, \quad (14)$$

where $\boldsymbol{\theta} = \text{column} [u, v, p]$, $\mathbf{F} = \text{column} [0, 0, F_p]$, and

$$L_1 = \begin{pmatrix} L_{xx} & 0 & -L_x \\ 0 & L_{xx} & 0 \\ -L_x & 0 & L_{xx} \end{pmatrix}, \quad L_2 = \begin{pmatrix} L_{yy} & 0 & 0 \\ 0 & L_{yy} & -L_y \\ 0 & -L_y & L_{yy} \end{pmatrix},$$

$$C_1 = \begin{pmatrix} -C_x & 0 & 0 \\ 0 & -C_x & 0 \\ 0 & 0 & 0 \end{pmatrix}, \quad C_2 = \begin{pmatrix} -C_y & 0 & 0 \\ 0 & -C_y & 0 \\ 0 & 0 & 0 \end{pmatrix},$$

$$F_p = \frac{1}{\text{Re}} \left(\frac{\partial C[u]}{\partial x} + \frac{\partial C[v]}{\partial y} \right),$$

$$L_{xx} = \frac{1}{\text{Re}} \frac{\partial^2}{\partial x^2}, \quad L_{yy} = \frac{1}{\text{Re}} \frac{\partial^2}{\partial y^2}, \quad L_x = \frac{\partial}{\partial x}, \quad L_y = \frac{\partial}{\partial y}. \quad (15)$$

Among the available operator-splitting schemes we generalize to the vectorial case the second Douglas scheme (see [16]) which is called also ‘‘stabilizing correction’’. It is of first order in time, but has some advantages in stability, especially for non-commuting operators (see [48]). The order of approximation with respect to the fictitious time is not important here as far as we are looking for the stationary solution after the time stepping (the iterations) converge.

For a generic vectorial system of the following type

$$I \frac{\partial \boldsymbol{\theta}}{\partial t} = (N_1 + N_2) \boldsymbol{\theta} + \mathbf{F}, \quad I \stackrel{\text{def}}{=} \begin{pmatrix} E & 0 & 0 \\ 0 & E & 0 \\ 0 & 0 & E \end{pmatrix}, \quad (16)$$

the scheme of stabilizing correction reads

$$\frac{\boldsymbol{\theta}^{n+1/2} - \boldsymbol{\theta}^n}{\tau} = N_1 \boldsymbol{\theta}^{n+1/2} + N_2 \boldsymbol{\theta}^n + \mathbf{F}^n, \quad \frac{\boldsymbol{\theta}^{n+1} - \boldsymbol{\theta}^{n+1/2}}{\tau} = N_2 (\boldsymbol{\theta}^{n+1} - \boldsymbol{\theta}^n), \quad (17)$$

where E is the unitary operator and τ is the increment of the fictitious time. Here N_1 and N_2 are difference approximations of the operators $L_1 + C_1$ and $L_2 + C_2$, respectively on a rectangular grid of size $N_x \times N_y$. Then the identity matrix I is of size $3 \times N_x \times N_y$.

Now Eq. (17) recasts as follows (for the scalar case, see, e. g. [41])

$$(I - \tau N_1) \boldsymbol{\theta}^{n+\frac{1}{2}} = (I + \tau N_2) \boldsymbol{\theta}^n + \tau \mathbf{F}^n, \quad (18)$$

$$(I - \tau N_2) \boldsymbol{\theta}^{n+1} = \boldsymbol{\theta}^{n+\frac{1}{2}} - \tau N_2 \boldsymbol{\theta}^n. \quad (19)$$

Acting upon (19) with the operator $(I - \tau N_1)$ and adding the result to (18) one gets

$$(I - \tau N_1) (I - \tau N_2) \boldsymbol{\theta}^{n+1} = -(I - \tau N_1) \tau N_2 \boldsymbol{\theta}^n + (I + \tau N_2) \boldsymbol{\theta}^n + \tau \mathbf{F}^n, \quad (20)$$

or which is the same,

$$[I + (\tau N_1)(\tau N_2)] (\boldsymbol{\theta}^{n+1} - \boldsymbol{\theta}^n) = (\tau N_1 + \tau N_2) \boldsymbol{\theta}^{n+1} + \tau \mathbf{F}^n, \quad (21)$$

and thus the intermediate variable $\boldsymbol{\theta}^{n+\frac{1}{2}}$ is eliminated

$$(I + \tau^2 N_1 N_2) \frac{\boldsymbol{\theta}^{n+1} - \boldsymbol{\theta}^n}{\tau} = (N_1 + N_2) \boldsymbol{\theta}^{n+1} + \mathbf{F}^n. \quad (22)$$

Due to the additions in the Poisson equation for pressure, the operator $L_1 L_2$ is positive definite (for the standard case of trivial b.c. for all of the unknown functions). This has an ameliorating impact on the stability of the splitting scheme making it absolutely stable in the sense that the false transient decays for any τ . The absolute stability is in place only for calculations that start from an initial condition close enough to the sought stationary solution. When the initial condition is not really close to the sought solution, then some mild limitations on the time step ensue.

Upon acknowledging the incompressibility constraint, $L_x u = -L_y v$, and specifying trivial b.c for the vectorial function, after some manipulations we obtain

$$(L_1 L_2 \boldsymbol{\theta}, \boldsymbol{\theta}) = \frac{1}{\text{Re}^2} \iint_{\Omega} [(L_x L_y u)^2 + (L_x L_y v)^2 + (L_x L_y p)^2] dx dy + \iint_{\Omega} (L_y v)^2 dx dy \geq \frac{m}{\text{Re}^2} (\boldsymbol{\theta}, \boldsymbol{\theta}), \quad m = m(\Omega) > 0. \quad (23)$$

Hence the operator $L_1 L_2$ is positive definite. (Note that for the last equality the imbedding theorem is used).

Since we invert here the operators N_1, N_2 rather than L_1, L_2 , the actual situation is more complicated. Yet, the positive-definiteness of $L_1 L_2$ secures that the addition of the term $-(u_x + v_y)$ in the Poisson equation for the pressure does not lead to additional terms in full-time steps after the fractional steps are eliminated. In other words the said addition does not diminish the stability of the *splitting* scheme. At this point this is an argument of heuristic nature which is *a-posteriori* vindicated by the practical comportment of the scheme as demonstrated in what follows.

5. Difference Approximations and Algorithm

The lid-driven flow occupies the region (the cavity)

$$\Omega = \{0 \leq x \leq 1, 0 \leq y \leq 1\}.$$

The boundary conditions for velocity components are

$$u(x, 0) = u(0, y) = u(1, y) = 0, \quad u(x, 1) = 1, \quad (24)$$

$$v(x, 0) = v(x, 1) = v(0, y) = v(1, y) = 0, \quad (25)$$

to which additional conditions stemming from (8) are added, namely

$$\left. \frac{\partial u}{\partial x} \right|_{(0,y)} = \left. \frac{\partial u}{\partial x} \right|_{(1,y)} = 0, \quad \left. \frac{\partial v}{\partial y} \right|_{(x,0)} = \left. \frac{\partial v}{\partial y} \right|_{(x,1)} = 0. \quad (26)$$

The mesh is staggered for u in x -direction x and for v in y -direction (see Fig. 1, *a*) which is consistent with other works on (u, v, p) formulation (see, e. g., [5]). For boundary conditions involving derivatives the staggered grid allows one to use central differences with second-order of approximation on two-point stencils.

The number of main grid lines (which are, in fact, the lines for the p -grid) in the x - and y -directions are respectively N_x and N_y . The numbers of intervals are $N_x - 1$ and $N_y - 1$. The spacings are given by:

$$h_x = \frac{1}{N_x - 1}, \quad h_y = \frac{1}{N_y - 1} \quad \text{and} \quad (x_i, y_j) = [(i - 1)h_x, (j - 1)h_y]$$

for $i = 1, \dots, N_x, j = 1, \dots, N_y$.

In Fig. 1, *b* the pressure is sampled at the points labeled by “•”; function u — at “○”; function v — at “*”. The following notations are used: $p_{i,j} = p(x_i, y_j)$, $u_{i,j} = u\left(x_i - \frac{1}{2}h_x, y_j\right)$, $v_{i,j} = v\left(x_i, y_j - \frac{1}{2}h_y\right)$.

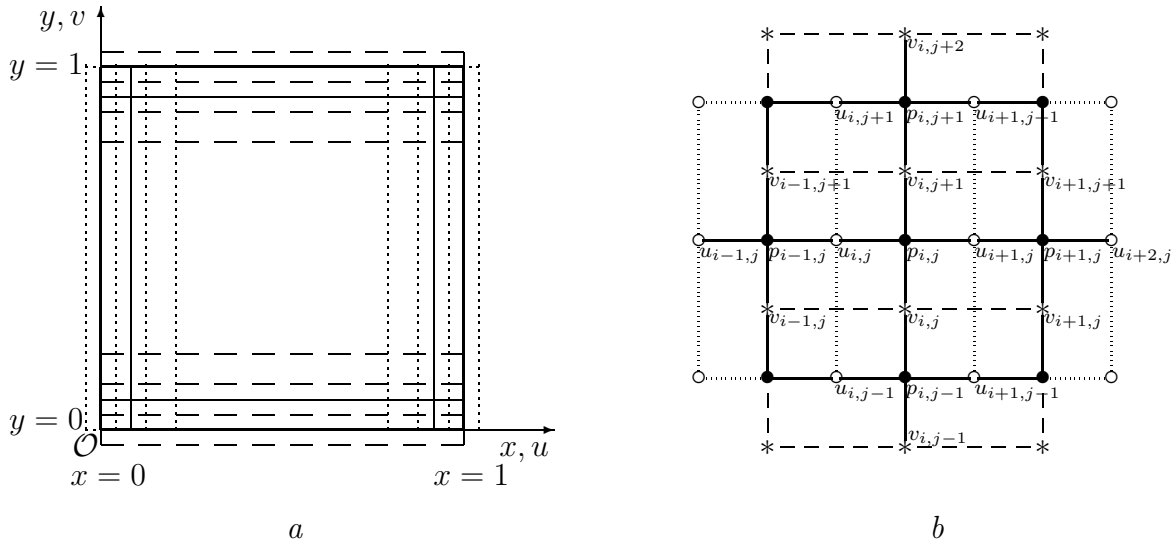


Fig. 1. The computational domain with the grid (a); the finite-difference stencil (b).

We employ second-order central-difference approximations for the operators in (17) which inherit the negative definiteness of the respective differential operators L_{xx} and L_{yy}

$$L_{xx}^h f = \frac{f_{i+1,j} - 2f_{i,j} + f_{i-1,j}}{\text{Re } h_x^2}, \quad L_{yy}^h f = \frac{f_{i,j+1} - 2f_{i,j} + f_{i,j-1}}{\text{Re } h_y^2}, \quad (27)$$

where f stands for one of the functions u , v , or p . The operators L_x and L_y are approximated with order $O(h_x^2 + h_y^2)$ in each of the interior mesh-points of the domain Ω , namely:

$$L_x^h p = \frac{p_{i,j} - p_{i-1,j}}{h_x}; \quad L_y^h p = \frac{p_{i,j} - p_{i,j-1}}{h_y}; \quad (28)$$

$$L_x^h u = \frac{u_{i+1,j} - u_{i,j}}{h_x}; \quad L_y^h v = \frac{v_{i,j+1} - v_{i,j}}{h_y}. \quad (29)$$

The operator F_p^h has the following form

$$\begin{aligned} F_p^h = & \frac{1}{\text{Re}} \left\{ \frac{1}{h_x^2} \left[\left(\frac{u_{i+2,j} + u_{i+1,j}}{2} \right)^2 - 2 \left(\frac{u_{i+1,j} + u_{i,j}}{2} \right)^2 + \left(\frac{u_{i,j} + u_{i-1,j}}{2} \right)^2 \right] + \right. \\ & + \frac{2}{h_x h_y} \left[\frac{(u_{i,j} + u_{i,j-1})(v_{i-1,j} + v_{i,j})}{4} - \frac{(u_{i+1,j} + u_{i+1,j-1})(v_{i,j} + v_{i+1,j})}{4} + \right. \\ & \left. \left. + \frac{(u_{i+1,j+1} + u_{i+1,j})(v_{i,j+1} + v_{i+1,j+1})}{4} - \frac{(u_{i,j+1} + u_{i,j})(v_{i-1,j+1} + v_{i,j+1})}{4} \right] + \right. \\ & \left. + \frac{1}{h_y^2} \left[\left(\frac{v_{i,j+2} + v_{i,j+1}}{2} \right)^2 - 2 \left(\frac{v_{i,j+1} + v_{i,j}}{2} \right)^2 + \left(\frac{v_{i,j} + v_{i,j-1}}{2} \right)^2 \right] \right\}. \end{aligned}$$

Note that the function u in the above formula is taken on the “old” time stage, i. e. u^n .

We consider the following second-order conservative approximations of the non-linear operators C_x and C_y which are akin to those proposed by Arakawa [3] for the $\psi - \omega$ formulation for ideal

flows. A similar idea in primitive variables was elaborated in [31] with a special reference to the operator-splitting schemes:

$$\begin{aligned}
 C_x^h[u] &= \frac{(u_{i+1,j}^n + u_{i,j}^n)u_{i+1,j} - (u_{i,j}^n + u_{i-1,j}^n)u_{i-1,j}}{4h_x}, \\
 C_y^h[u] &= \frac{(v_{i,j+1}^n + v_{i-1,j+1}^n)u_{i,j+1} - (v_{i,j}^n + v_{i-1,j}^n)u_{i,j-1}}{4h_y}, \\
 C_x^h[v] &= \frac{(u_{i+1,j}^n + u_{i+1,j-1}^n)v_{i+1,j} - (u_{i,j}^n + u_{i,j-1}^n)v_{i-1,j}}{4h_x}, \\
 C_y^h[v] &= \frac{(v_{i,j+1}^n + v_{i,j}^n)v_{i,j+1} - (v_{i,j}^n + v_{i,j-1}^n)v_{i,j-1}}{4h_y}.
 \end{aligned} \tag{30}$$

Here the superscript n stands for the previous (“old”) time stage. The functions without superscript can be taken either on the “new” time stage ($n + 1$) or on the old one according to the difference scheme. Thus the functions u, v in the nonlinear term are treated as known (“frozen”) coefficients while their derivatives (finite differences) are the yet unknown values from the current (“new”) time stage.

It is readily shown that the discrete operators C_x^h and C_y^x preserve the skew-symmetric property of the differential operators C_x and C_y and hence

$$(C_x^h[u], u) = 0, \quad (C_y^h[u], u) = 0, \quad (C_x^h[v], v) = 0, \quad (C_y^h[v], v) = 0,$$

where the ubiquitous scalar product,

$$(\alpha, \beta) = \sum_i \sum_j \alpha_{i,j} \beta_{i,j} h_x h_y,$$

is used and the appropriate boundary conditions are acknowledged.

Using the approach of [3, 31] allows one to end up with a scheme free of artificial viscosity. An illuminating discussion on the quantitative effects of the scheme viscosity can be found in [15] for the lid-driven cavity flow.

The scheme proposed here allows a very efficient treatment of the algebraic systems. On each fractional time-steps two systems are to be solved. One of them is a coupled system for respective velocity component and the pressure while the other is a decoupled system for the remaining velocity component. For instance, on the first half-time stage the x -operators are inverted along the line $y = y_j$ where u and p are conjugated, and v is decoupled from them. As a result, two linear algebraic systems are to be solved numerically: one for the set function

$$\mathbf{v}^{n+\frac{1}{2}} = \text{column} \left[v_{1,j}^{n+\frac{1}{2}}, \dots, v_{i,j}^{n+\frac{1}{2}}, \dots, v_{N_x,j}^{n+\frac{1}{2}}, v_{N_x+1,j}^{n+\frac{1}{2}} \right]$$

with tridiagonal matrix (for definiteness, call it \mathcal{A}_v), and another — for the “composite” difference function

$$\mathbf{w}^{n+\frac{1}{2}} = \text{column} \left[u_{1,j}^{n+\frac{1}{2}}, p_{1,j}^{n+\frac{1}{2}}, \dots, u_{i,j}^{n+\frac{1}{2}}, p_{i,j}^{n+\frac{1}{2}}, \dots, u_{N_x,j}^{n+\frac{1}{2}}, p_{N_x,j}^{n+\frac{1}{2}}, u_{N_x+1,j}^{n+\frac{1}{2}} \right]$$

which turns out to be a pentadiagonal matrix twice the size of the tridiagonal one (call it \mathcal{A}_{up} for definiteness). For the grid line $y = y_j$, the two linear algebraic systems can be rewritten in the form:

$$\mathcal{A}_{up} \cdot \mathbf{w}^{n+\frac{1}{2}} = \mathcal{R}_{up}, \quad \mathcal{A}_v \cdot \mathbf{v}^{n+\frac{1}{2}} = \mathcal{R}_v. \tag{31}$$

In the same manner, the second half time-step along the line $x = x_i$ requires solving a tridiagonal system for the set function

$$\mathbf{u}^{n+1} = \text{column} \left[u_{i,1}^{n+1}, \dots, u_{i,j}^{n+1}, \dots, u_{i,N_y}^{n+1}, u_{i,N_y+1}^{n+1} \right]$$

and a pentadiagonal system for the “composite” set function

$$\mathbf{z}^{n+1} = \text{column} \left[v_{i,1}^{n+1}, p_{i,1}^{n+1}, \dots, v_{i,j}^{n+1}, p_{i,j}^{n+1}, \dots, v_{i,N_y}^{n+1}, p_{i,N_y}^{n+1}, v_{i,N_y+1}^{n+1} \right],$$

namely

$$\mathcal{B}_u \cdot \mathbf{u}^{n+1} = \mathcal{S}_u, \quad \mathcal{B}_{vp} \cdot \mathbf{z}^{n+1} = \mathcal{S}_{vp}. \quad (32)$$

We solve the above banded systems by means of a specialized Gaussian-elimination solver [8] employing pivoting which is a generalization of what in the tridiagonal case is known as Thomas algorithm in the English-language literature or “*progonka*” — in the Russian-language literature. Any other solver will do the job too. Our specialized solver is somewhat faster for the banded systems under consideration whose number of diagonals is relatively small.

The general sequence of the algorithm is as follows

- (i) Set the values of Re , τ , ε , N_x , N_y and choose an initial guess $u_{i,j}^0$, $v_{i,j}^0$, $p_{i,j}^0$.
- (ii) Consider $u_{i,j}^n$, $v_{i,j}^n$, $p_{i,j}^n$ as known entities and calculate the difference functions $u_{i,j}^{n+\frac{1}{2}}$, $v_{i,j}^{n+\frac{1}{2}}$, $p_{i,j}^{n+\frac{1}{2}}$ from the equations (31) for the first fractional time-step.
- (iii) Using $u_{i,j}^n$, $v_{i,j}^n$, $p_{i,j}^n$ and $u_{i,j}^{n+\frac{1}{2}}$, $v_{i,j}^{n+\frac{1}{2}}$, $p_{i,j}^{n+\frac{1}{2}}$ as known entities, calculate the values $u_{i,j}^{n+1}$, $v_{i,j}^{n+1}$, $p_{i,j}^{n+1}$ from the equations (32) for the second fractional time-step. Set $p_{i,j}^{n+1} := p_{i,j}^{n+1} - \hat{p}^{n+1}$, where \hat{p}^{n+1} is the average of the pressure¹.
- (iv) If the following criterion is satisfied

$$\max\{R^u(n), R^v(n), R^p(n)\} \leq \varepsilon, \quad \text{where} \quad R^f(n) \stackrel{\text{def}}{=} \frac{\max_{i,j} |f_{i,j}^{n+1} - f_{i,j}^n|}{\tau \max_{i,j} |f_{i,j}^{n+1}|}, \quad (33)$$

then the calculations are terminated. Otherwise the index of iterations is stepped up $n := n + 1$ and the algorithm is returned to step (ii).

6. Numerical Results for Lid-Driven Cavity Flow

A numerical treatment of the lid-driven cavity flow appeared as early as in 1966 [6] featuring reliable results up to $\text{Re} = 400$. Since then it received enormous attention and has become a benchmark test for any new algorithm for N-S equations.

For this particular flow problem when $\text{Re} \leq 10000$, a plethora of published results are available for from a number of sources [11, 21, 28, 43, 46, 19, 14, 36], but the accuracy of some of these solutions has generally been regarded with certain skepticism because of the sizes of the computational grids involved and the difficulties connected with the convergence when the dissipation was very small (high Reynolds numbers). Exception to these may be the results [18]

¹In incompressible flows the pressure is defined up to an arbitrary function of time. For the sake of convenience we define this function similarly to [1, 2] as the spatial average of the pressure at the specific time stage.

and [44] which were obtained employing multigrid and finite-element techniques, respectively. Because of the specifics of the finite-difference methods, we will compare our results mostly with the highly accurate solutions presented in [18] for grids with up to 256×256 grid cells. Various physical characteristics are computed in the present section and shown to be in very good quantitative agreement with the literature.

6.1. Consistency and Convergence

For the difference solution presented here, there exist two main sources of computational errors. The first is the truncation error which is defined *a-priori* by the type of approximation and in the present paper it is of order $O(h^2)$. The truncation error does not depend on the way the iterations are conducted. The second cause is the artificial time derivative which is supposed to vanish as the “false transient” decays. This error can be controlled *a-posteriori* by means of varying the tolerances ε used to terminate the iterations. In our definition (33) for the tolerances, the time increment τ is in the denominator hence $R^f(u)$, etc., are measures of the relative contributions of the artificial time derivatives to each of the equations. It is clear that there is no justification to take ε much smaller than the truncation error which is of order $O(h^2)$. Since the finest grid used in the present paper has 512×512 cells then $h^2 \approx 4 \cdot 10^{-6}$. For a reliable control of the convergence (the decay of the “false transient”) we select $\varepsilon = 10^{-6}$. Strictly speaking this value is an overkill and is near the margin of the possible accuracy with double precision. It is interesting to mention here that the predominant part of the iterations (about 60 %) are spent to time-step the process from $\varepsilon = 10^{-5}$ to $\varepsilon = 10^{-6}$.

We conducted extensive numerical experiments with the above proposed scheme and algorithm. The calculations in the present subsection are aimed to study the consistency of the scheme for different spatial resolutions as well as the dependence of the solution and the rate of convergence on the mesh size h , Reynolds number Re , and fictitious-time increment τ . In order to interrogate the accuracy and efficiency of the scheme we consider equal spacings in the two directions $h_x = h_y = h$ and obtain the solution on six different grids: $h^{-1} = 16, 32, 64, 128, 256, 512$ and with various time increments τ .

For $\varepsilon = 10^{-6}$ and fixed values of h and Re , the number of iterations needed for convergence (terminal number of iterations) depends on τ . It is of primary interest to estimate the optimal range of τ in which the convergence is fastest, i. e. when the terminal number of iterations is the least. For definiteness we select for presentation a genuinely moderate Reynolds number $Re = 1000$ and vary the spacing h . The results for the terminal number of iterations for this set of parameters is shown in Table 1 where the minimal terminal number for each resolution is shown in bold face. As it should have been expected the optimal value for τ is roughly proportional to \sqrt{h} but the dependence of the actual terminal number N on h is much weaker. For practical purposes one can assume that the optimal time increment lies in the interval $\tau \in [0.05, 0.2]$ and be prepared to perform of order of 1000 iterations for convergence.

The results confirm the full approximation of the scheme (no dependence of the steady-state solution on the magnitude of time increment τ). Juxtaposition of the results with different grids confirm the $O(h^2)$ spatial approximation.

For very high Reynolds numbers the terminal number of iterations increases more than an order of magnitude.

6.2. Comparisons for the Velocity Components

Because of the nonlinearity of the Navier—Stokes equations and the implicit nature of the continuity condition, the practical approximation of any scheme can turn out to be rather

T a b l e 1

The terminal number of iterations
for $\text{Re}=1000$, $\varepsilon=10^{-6}$ and different τ, h

$1/h$	τ						
	0.01	0.02	0.05	0.10	0.20	0.40	0.80
16	8552	4816	2236	1275	795	635	1711
32	7498	4383	2051	1175	742	1279	2856
64	6634	3835	1883	1072	897	1846	3706
128	6472	3533	1718	1029	1189	2336	4472
256	6490	3444	1688	1024	1534	2883	5347
512	6503	3377	1686	1230	2258	4120	7437

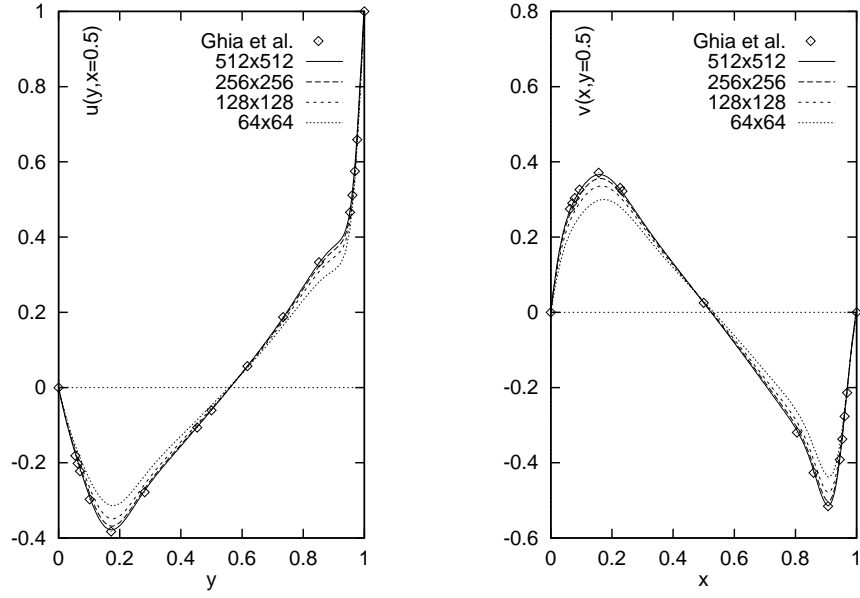
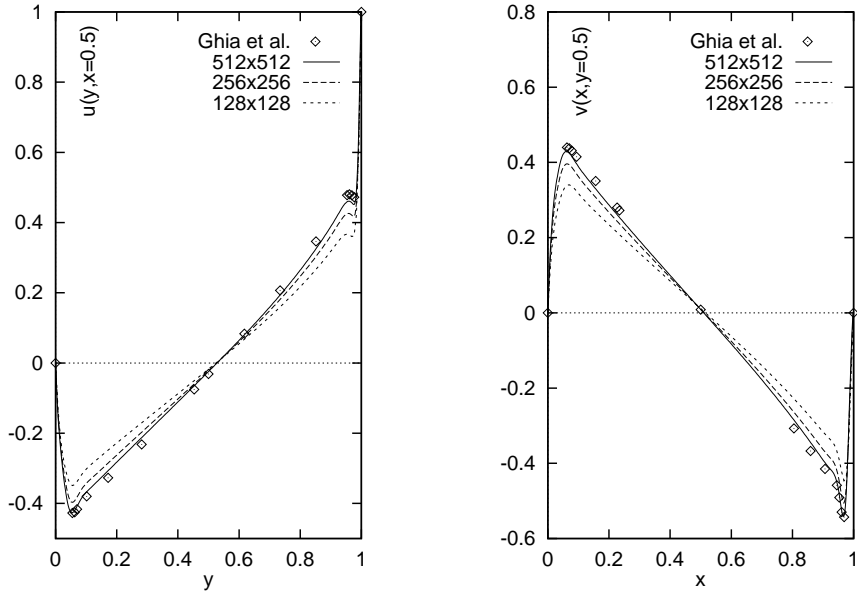
different from the theoretical estimates. This is especially true for very high Reynolds numbers. Different schemes perform better in different situations. No single scheme can be best in all instances. That is why in the last several years new schemes have appeared on ever increasing pace.

Insofar as we employ primitive variables, the most natural characteristics to compare are the velocity components and the pressure.

We begin with the velocity profiles for the horizontal and vertical lines through the geometrical center of the cavity. The profiles of u along the vertical cross section and v — along the horizontal cross section are shown in Fig. 2 for $\text{Re} = 1000$ on different grids. They are in close agreement between themselves and the three finest grids clearly demonstrate the $O(h^2)$ approximation of the scheme (note that our scheme is free from artificial viscosity). In the same Fig. 2 we include also the velocity components as calculated in [18]. The agreement is very good, even better than it should have been expected if one takes into account the fact that the single-grid scheme used in [18] for this particular Reynolds number is an upwind scheme on grid of 128×128 cells, i. e. $h \approx 0.008$. This gives a rough estimate for the truncation error in [18] which is supposed to be of order of the so-called “cell” Reynolds number $O(h\text{Re})$. Thus one arrives at an estimate for the truncation error which is formally greater than unity in this particular case (grid of 128 intervals). Yet, the results of [18] are in excellent quantitative agreement with our finest mesh. It is clear that the good performance of the scheme [18] is a result of the multigrid approach taken in that work. We were not able to find in the text of [18] the details of how the multigrid results were used to increase the overall accuracy of the solution, but it is clear that the final solution there is of order of $O(h^4)$ and compares very well with our Richardson extrapolation of order $O(h^4)$ on the grid of 256×256 cells. Fig. 3 testifies to the same behaviour of the results for a very large Reynolds number $\text{Re} = 10000$.

6.3. Comparisons for the Stream Function

The majority of the papers deal with stream function formulations and the most popular elements of the fine structure of the flow to be compared are the characteristics of the local vortices. These correspond to the local extrema of the stream function. In order to make comparison for the stream and vorticity functions we need to calculate them after the iterative process for u, v , and p converges. From the velocity components on the respective staggered grids, then we calculate the discrete vorticity function $\omega_{i,j}$ on the main grid according to the


 Fig. 2. Velocity profiles through the cavity center, $Re = 1000$.

 Fig. 3. Velocity profiles through the cavity center, $Re = 10000$.

following formula

$$\omega_{i,j} \stackrel{\text{def}}{=} v_x - u_y = \frac{[(v_{i+1,j+1} + v_{i,j+1} + v_{i,j} + v_{i+1,j}) - (v_{i,j+1} + v_{i,j} + v_{i-1,j} + v_{i-1,j+1})]}{4h_x} - \frac{[(u_{i+1,j+1} + u_{i,j+1} + u_{i,j} + u_{i+1,j}) - (u_{i+1,j} + u_{i,j} + u_{i,j-1} + u_{i+1,j-1})]}{4h_y}. \quad (34)$$

and solve for the stream function the respective Poisson equation $-\Delta\psi = \omega$.

The particular method and algorithm are of no relevance to the main narrative of the present paper. Therefore their discussion is omitted for the sake of conciseness of the text. We only

mention that we use a standard splitting scheme [16] but now for the ubiquitous second-order parabolic equation.

The tolerance level for convergence is set to the same value $\varepsilon = 10^{-6}$, so that the solution for ψ has the same accuracy as the solution for u, v , and p . A Richardson extrapolation is performed from the two finest grids 256 and 512 and used for all of the different calculations presented henceforth.

The streamline contours for different Re ranging from 1000 to 10 000 are shown in Fig. 4. For moderate Re these patterns consist of a primary vortex and secondary vortices. Tertiary vortices form with the increase of Re . In order to make the presentation uniform we use three sets of isolines representing the typical magnitudes of the stream function in the different parts of the flow (the sub-domains occupied by the different vortices). The different groups are marked with different lines: solid, dashed, and dotted. The magnitudes (the “numbers”) of the isolines are listed in the figure captions.

The accurate calculation of the magnitudes and locations of the centers of the primary, secondary, and tertiary vortices is one of the hardest tests. Taking merely the maximal/minimal values of the difference stream function gives rather crude values for the magnitudes and coordinates of the vortex centers. In the present work we took special care in handling the problem. After a local extremum of the stream function is located on the grid a 9-point stencil is formed with the extremum in its central point. Then the stream function ψ is approximated with 2D second-order polynomials on the stencil with third order of approximation. Upon setting the partial derivatives equal to zero a more accurate location of the vortex (extremum) is calculated. After that the amplitude of the vortex is calculated from the polynomial in that location.

The location of the center of the primary vortex as function of Reynolds number is shown in the upper panel of Fig. 5 while a similar result for the most intensive secondary vortex in the bottom right region is depicted in the lower panel of the same figure. Our results are compared to some of the literature sources. It is clearly seen that our curves are self-consistent and monotone while the literature data is more scattered. The interesting observation is that the scheme [36] which is off up to 30 % for the amplitude of the stream function gives relatively good prediction for the centers. This means that it has very low phase error. Our ongoing work [13] seems to support the same conjecture that the approximations employing stream-function formulation may be subject to smaller phase errors. Even the overall accurate results of [18] are subject to the same difficulties as the other papers from the literature when it comes to these fine-structure characteristics.

The scenario of appearance of the secondary and the tertiary vortices is qualitatively well established in the literature. The vortex in the bottom right corner first appears for $Re \approx 100$. The bottom left corner is occupied by another secondary vortex for $Re \approx 400$ and it remains less intensive than the bottom right vortex for all Reynolds numbers. With the increase of Re the center of the primary vortex shifts towards the geometric center of the cavity. This kind of behaviour is connected with the development of an inviscid core of the flow and boundary layers near the walls. As shown in Fig. 5, *b*, the position of the bottom right vortex is also a function of Reynolds number. Its center shifts to the central vertical cross-section with the increase of Re .

Table 2 summaries the data concerning the location and strengths of the primary vortex and the most significant secondary vortex in the bottom right corner. The results are compared with [46] (320×320 grid cells), [18] (multigrid solution), [11, 36] (stream function formulation), [4, 33] (non-uniform grid), [5], and some other difference solutions.

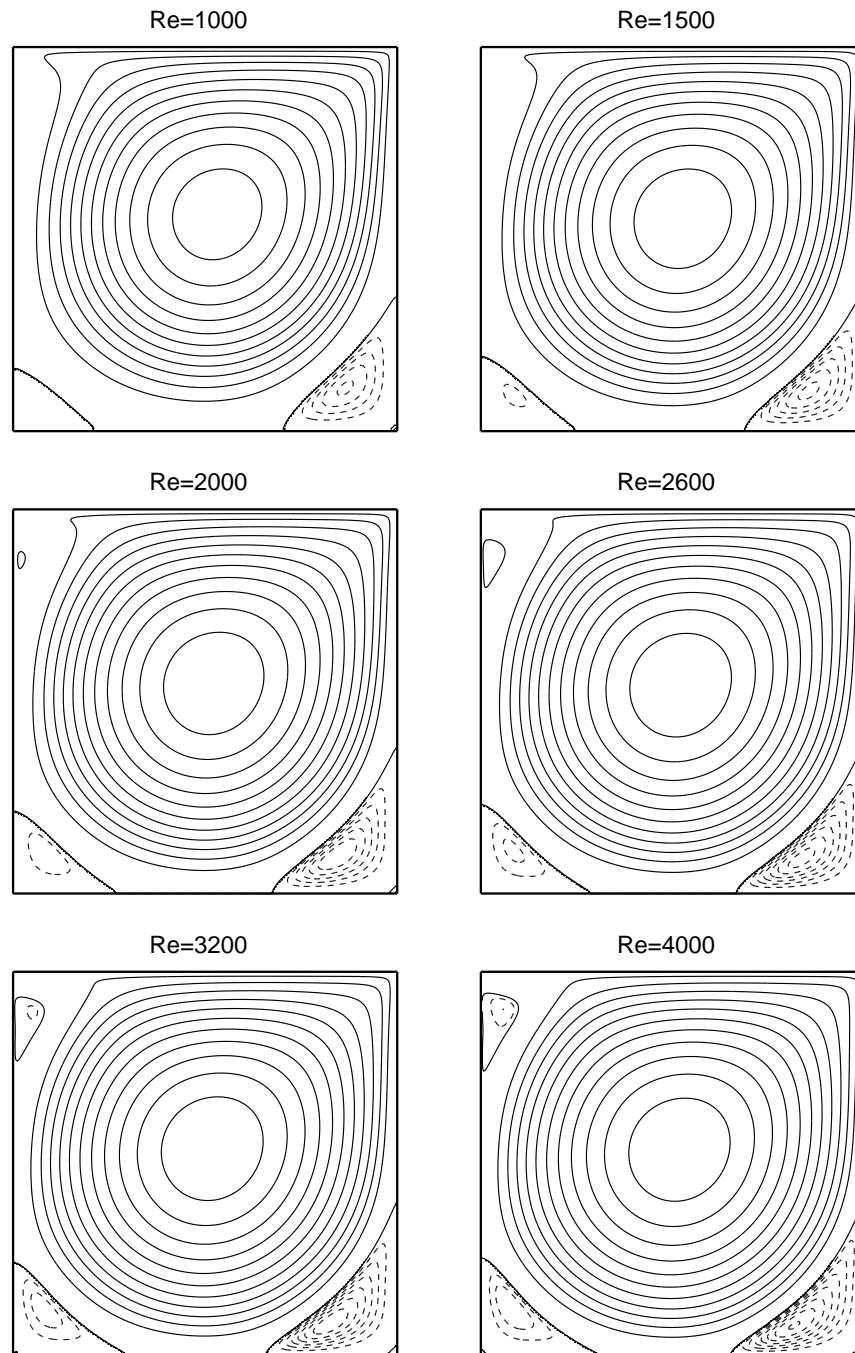


Fig. 4. Streamline patterns. Contour values are: — beginning from zero with increment -0.01 ; --- beginning from $+0.0004$ with increment 0.0004 ; - - - - beginning from $+0.0001$, with increment $+0.0001$; $\cdots\cdots\cdots$ beginning from -0.00002 with increment -0.00002 .

The qualitative evolution of the bottom-left secondary vortex with Re is rather similar to the secondary vortex in the bottom right corner and will not be discussed here in order not to overload the text.

The last of the secondary vortices to appear with the increase of Re is the one near the top-left corner of the cavity. It is more intricate in shape because of its close interaction with the discontinuity of the u component in the corner where the lid touches the left vertical wall. Unlike the other secondary vortices it does not occupy the corner itself. The value of Reynolds

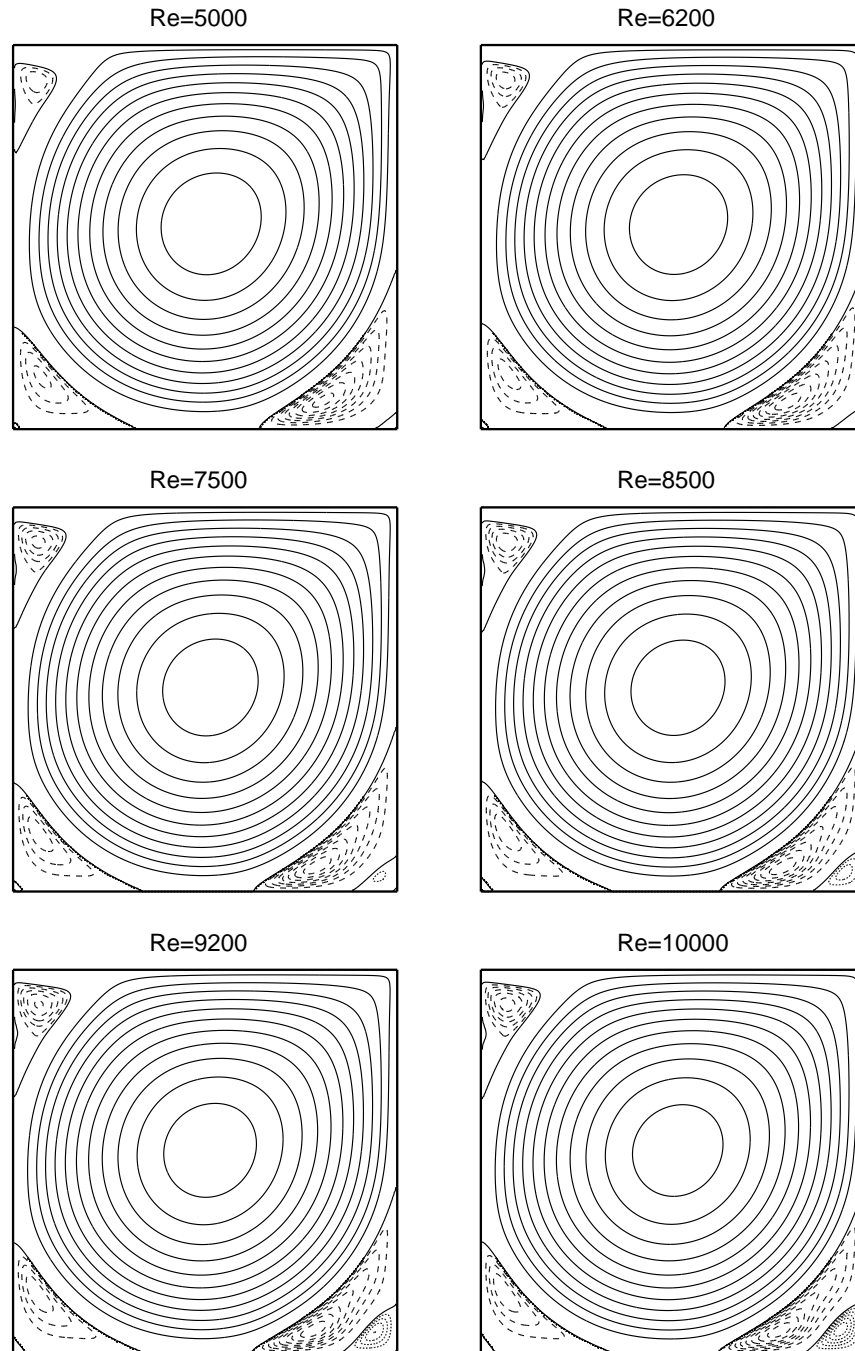


Fig. 4. (Continuation).

number for which it first appears is one of the important parameters for which there is no good quantitative data in the literature. In our calculation a faintest trace of positive circulation in the top-left region first showed up for $Re = 2000$. To get an idea of how the shape of top-left secondary vortex depends on Re we conducted special set of calculations which are presented in Fig. 6. Unlike the bottom right and bottom left secondary vortices the amplitude of top left secondary vortex keeps increasing with the increase of the Reynolds number. In this instance the results of [18] are in closer agreement with our results while the top-left secondary vortex of [15] is somewhat more developed for $Re = 2000$.

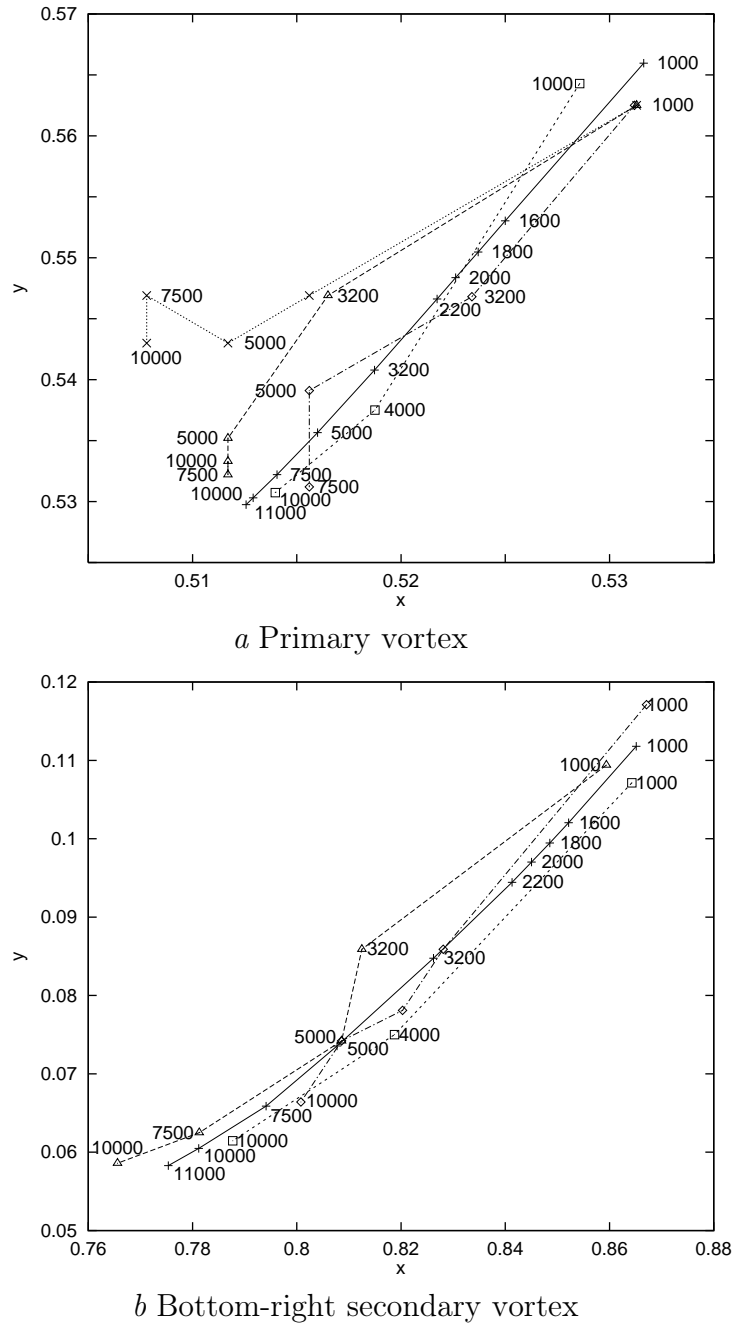


Fig. 5. Effect of Re on the location of vortex centers: $- + -$ present results; Δ [18] for $Re = 1000, 3200, 5000, 7500, 10\ 000$; \square [36] for $Re = 1000, 4000, 10\ 000$; \times [29].

A detectable tertiary vortex first appear in the bottom-right corner of the cavity for $Re \approx 5000$ and in the bottom-left corner for $Re \gtrsim 7500$. Scrutinizing our numerical results we discovered that tertiary negative vortices of magnitude 10^{-7} are always present (for all Reynolds numbers) in the lower corners. Yet such a magnitude is much bellow the threshold of the truncation error and/or the convergence tolerance ε . Hence the presence of a tertiary vortex of amplitude lesser than ε cannot be really verified as a physical characteristics. The tertiary vortices in the bottom corners persist for different grids and are consistent with the calculations in stream-function formulation [11].

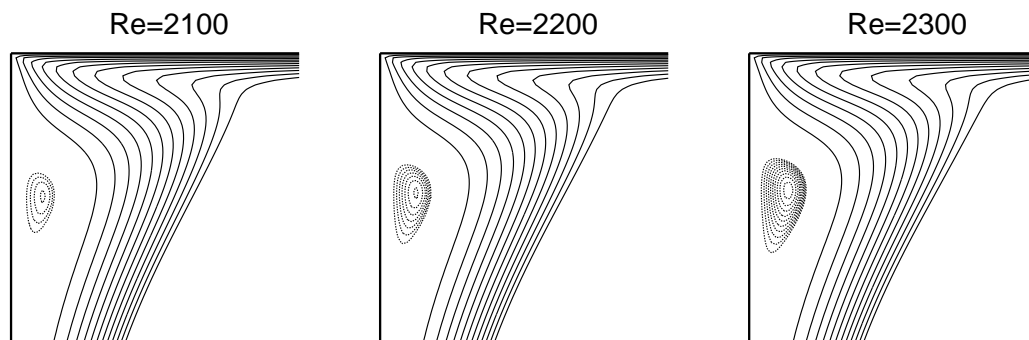


Рис. 6. The secondary vortex in the top-left corner for those Re when it first appears. Contour values are: — beginning from -0.001 with increment -0.001 ; $\cdots\cdots$ beginning from 0.00001 with increment 0.00001 .

An interesting issue is the appearance of still another tertiary vortex in the top left corner of the cavity for $Re = 8500 - 10\,000$. This tertiary vortex has not been observed in [18, 29, 36]. It is rather small and of very low intensity. We observe it only after the accuracy of the solution is increased to $O(h^4)$ through Richardson extrapolation. In our opinion the advent of that particular tertiary vortex marks the limit of the laminar flow. The conjunctions of secondary/tertiary vortices (and for higher Re quaternary vortices) in the top-left corner look much more as a stationary version of the Tollmin-Schlichting wave in the boundary layer near the walls. This ansatz, however, remains to be proved.

The vorticity contours are presented in Fig. 7. The equivorticity plots at high Reynolds numbers ($Re \geq 3200$) show a central region of nearly constant vorticity which form an inviscid core we mentioned in the precedence. It is surrounded by a nearly circular, thin region of flow of opposite vorticity (the boundary layer).

In a similar fashion Fig. 8 presents pressure contours. The data in the literature for the pressure isolines (called “isobars” in meteorology) is generally scant. The works [1, 2] for $Re \leq 400$ and [33] for $1000 \leq Re \leq 10\,000$ are the only ones we found in which isobars are plotted. The comparison with [33] appear to be in exact qualitative agreement in the sense of the position of centers of low and high pressure. The quantitative agreement is also very good.

6.4. Empirical Correlations for the Vortex Characteristics

The reliable results we obtained prompted us to arrange them in somewhat more user-friendly manner. We found best-fit formulas consisting predominantly of the simplest fractional powers of Reynolds number. The benefits of such a representation are twofold. First, it is very succinct and allows other investigators to compare to our results even for Reynolds numbers that are not among the main set of numerical experiments. Second, it gives clues for the boundary-layer models of the lid-driven cavity flow.

In Fig. 9 are shown the intensities (magnitudes) and the x - and y -coordinates of centers for the primary vortex, the bottom-right, bottom-left, and top-left secondary vortices, as well as for the bottom-right tertiary vortex. The simple empirical correlations we found to fit best the data are also included in the drawings and the captions making the Figure self-explanatory.

6.5. The Twilight Zone Beyond $Re \approx 10\,000$

A consensus has almost been reached by now that beyond $Re \approx 10\,000$ the dynamics of the lid-driven cavity flow changes. Curiously enough, this value of the Reynolds number is almost the same for the different iterative methods (e. g., of type of false transients [11, 30, 39]) and for

Table 2

Coordinates of the extrema of the stream function

Re	Ref. data	1/h	Primary vortex		Right-Bottom Vortex	
			ψ_{\min}	(x_{\min}, y_{\min})	ψ_{\max}	(x_{\max}, y_{\max})
1000	CM	512	-0.116269	(0.5316, 0.5660)	0.001640	(0.8651, 0.1118)
	CM	R 256	-0.116915	(0.5313, 0.5664)	0.001666	(0.8672, 0.1133)
	[4]	100	-0.1175		0.001724	
	[5]	64	-0.1163	(0.5313, 0.5586)	0.00191	(0.8711, 0.1094)
	[11]	80	-0.118710	(0.5346, 0.5645)		
	[18]	MG 128	-0.117929	(0.5313, 0.5625)	0.001751	(0.8594, 0.1094)
	[19]	128	-0.1157	(0.5312, 0.5625)	0.00163	(0.8671, 0.1171)
	[23]	FO 40	-0.111492	(0.475, 0.575)	0.001833	
	[29]		-0.1160	(0.5313, 0.5625)		
	[33]	NU 64	-0.118		0.00177	
[36]	180	-0.116030	(0.5286, 0.5643)	0.001700	(0.8643, 0.1071)	
[46]	320	-0.117300	(0.5438, 0.5625)	0.001740	(0.8625, 0.1063)	
2000	CM	512	-0.117198	(0.5226, 0.5484)	0.002353	(0.8450, 0.0970)
	CM	R 256	-0.118874	(0.5234, 0.5469)	0.002397	(0.8438, 0.0977)
	[11]	80	-0.112230	(0.5228, 0.5508)		
	[46]	320	-0.111600	(0.5250, 0.5500)	0.002600	(0.8375, 0.0938)
3200	CM	512	-0.116410	(0.5187, 0.5408)	0.002676	(0.8262, 0.0847)
	CM	R 256	-0.119257	(0.5195, 0.5391)	0.002726	(0.8281, 0.0859)
	[4]	100	-0.1210		0.002807	
	[18]	MG 128	-0.120377	(0.5165, 0.5469)	0.003140	(0.8125, 0.0859)
	[19]	128	-0.1122	(0.5234, 0.5468)	0.00262	(0.8281, 0.0859)
[29]		-0.1168	(0.5156, 0.5469)			
5000	CM	512	-0.116120	(0.5160, 0.5357)	0.002890	(0.8077, 0.0736)
	CM	R 256	-0.118047	(0.5156, 0.5352)	0.002940	(0.8086, 0.0742)
	[11]	80	-0.126610	(0.5062, 0.5232)		
	[18]	MG 256	-0.118966	(0.5117, 0.5352)	0.003084	(0.8086, 0.0742)
	[19]	256	-0.1115	(0.5156, 0.5391)	0.00299	(0.8086, 0.0742)
	[29]		-0.1186	(0.5117, 0.5430)		
	[33]	NU 64	-0.117		0.00299	
7500	CM	512	-0.113472	(0.5141, 0.5322)	0.003022	(0.7946, 0.06587)
	CM	R 256	-0.115282	(0.5137, 0.5321)	0.003069	(0.7932, 0.06588)
	[5]	256	-0.1113	(0.5156, 0.5234)	0.00832	(0.8828, 0.0820)
	[18]	MG 256	-0.119976	(0.5117, 0.5322)	0.003285	(0.7813, 0.0625)
	[19]	256	-0.1052	(0.5156, 0.5312)	0.00306	(0.8008, 0.0664)
	[29]		-0.1201	(0.5078, 0.5469)		
10 000	CM	512	-0.113848	(0.5129, 0.5303)	0.003010	(0.7812, 0.0605)
	CM	R 256	-0.116470	(0.5125, 0.5302)	0.003050	(0.7787, 0.0602)
	[4]	150	-0.1211		0.003270	
	[5]	256	-0.1053	(0.5156, 0.5234)	0.00986	(0.8495, 0.0820)
	[18]	MG 256	-0.119731	(0.5117, 0.5333)	0.003418	(0.7656, 0.0586)
	[29]		-0.1201	(0.5078, 0.5430)		
[36]	180	-0.102840	(0.5140, 0.5307)	0.002960	(0.7877, 0.0614)	
11 000	CM	512	-0.113394	(0.5126, 0.5298)	0.002977	(0.7754, 0.0583)

MG — Multigrid solution; NU — non-uniform grid; FO — Fourth order scheme;

R — Richardson extrapolation from solutions 256 and 512; CM — present results.

the genuinely unsteady calculations, as well. Beyond that threshold a non-steady régime takes place. The interesting thing is that the unsteady flow do not immediately becomes a turbulent one. It is more like a steady flow with small amplitude oscillatory motion superimposed on it. The results of [5] show that for $Re = 7500, 10\,000, 11\,000$ small tertiary vortices appear and

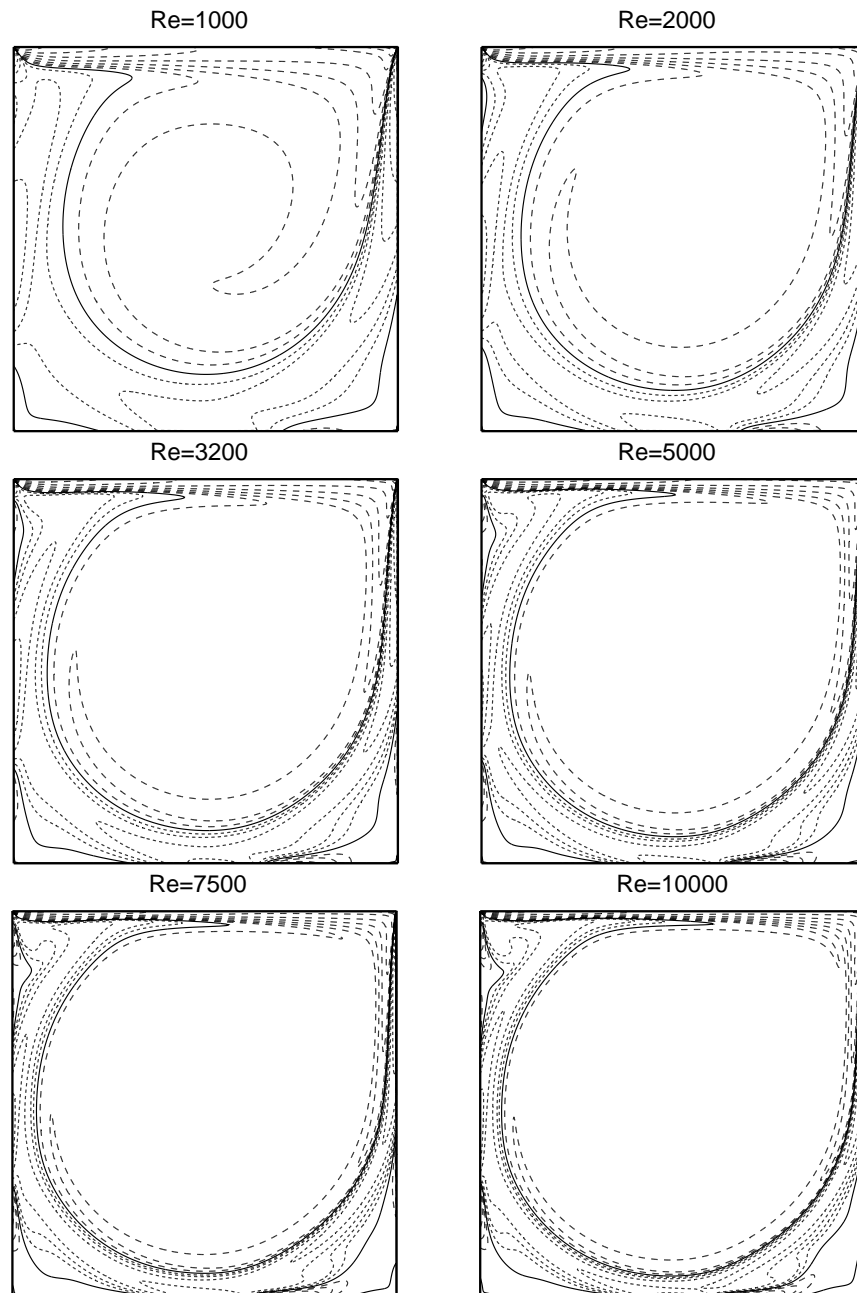


Рис. 7. Vorticity isolines: — — — -1, -2, -4, -8, -16, -32, -64, -128, -256, -512, -10244; ——— 0; - - - - 1, 2, 4, 8, 16, 32, 64, 128.

disappear in oscillatory fashion in the regions occupied by the secondary ones. That is why some investigators speak about Hopf bifurcation. In a different, though rather similar situation (wind driven flow), a behaviour resembling Hopf bifurcation was observed in [37] for Re up to 14 000.

In the light of the comments in the previous subsection about the multigrid and Richardson extrapolation, a simple conjecture is in place. Just like the artificial viscosity (arising in up-wind approximations of the advective terms) acts to unrealistically smooth the solution, the artificial dispersion of order $O(h^2\text{Re})$, stemming from the higher-order terms in the truncation error for the advection, acts to introduce artificial waves. In most of the high-quality algorithms the artificial viscosity is either very low or absent so that it takes a long time for the artificially

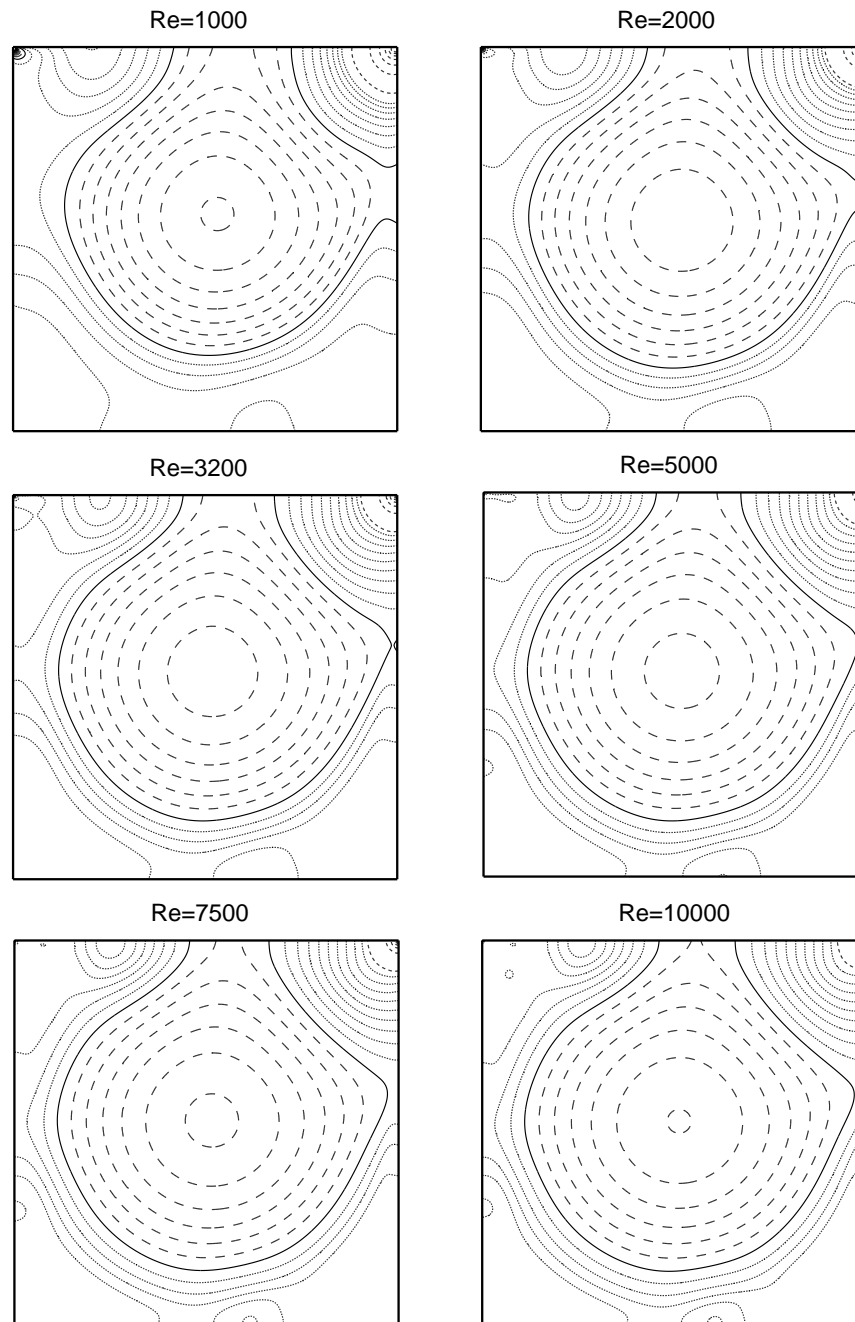


Рис. 8. Pressure isolines: — $p = 0$., - - - beginning from -0.01 with spacing -0.01 ; ···· beginning from 0.1 with spacing 0.1 ; · · · · beginning from 0.01 with spacing 0.01 .

excited waves to dissipate. In our opinion, a multigrid solution of the type of [18] or a Richardson approximation on two different grids remain the two most viable options for reliable numerical prediction at very high Reynolds numbers.

Because of the artificial dispersion of the schemes without multigrid and/or Richardson extrapolation one can never be sure whether the oscillations are purely numerical effect or they reflect certain physical mechanism of transition to an irregular régime in the lid-driven flow. In this connection the false-transient methods like the one presented here can still reach a steady solution (albeit after long meandering in the functional space) while the real physical

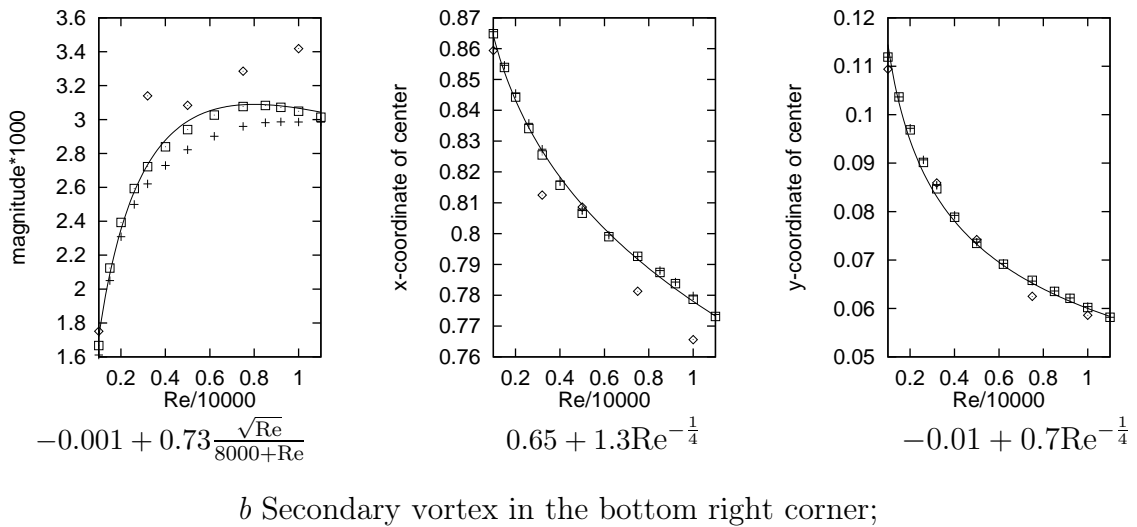
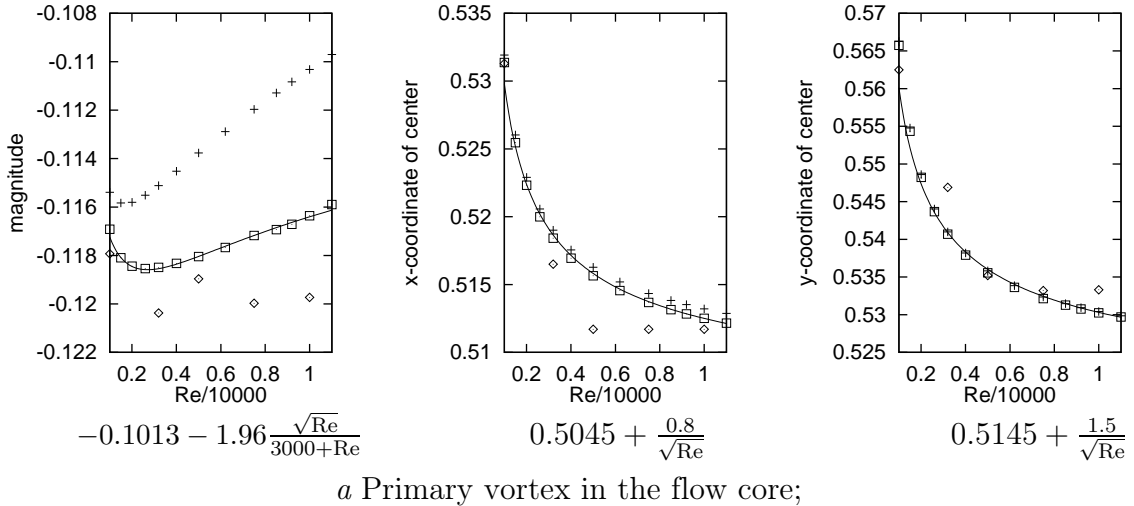


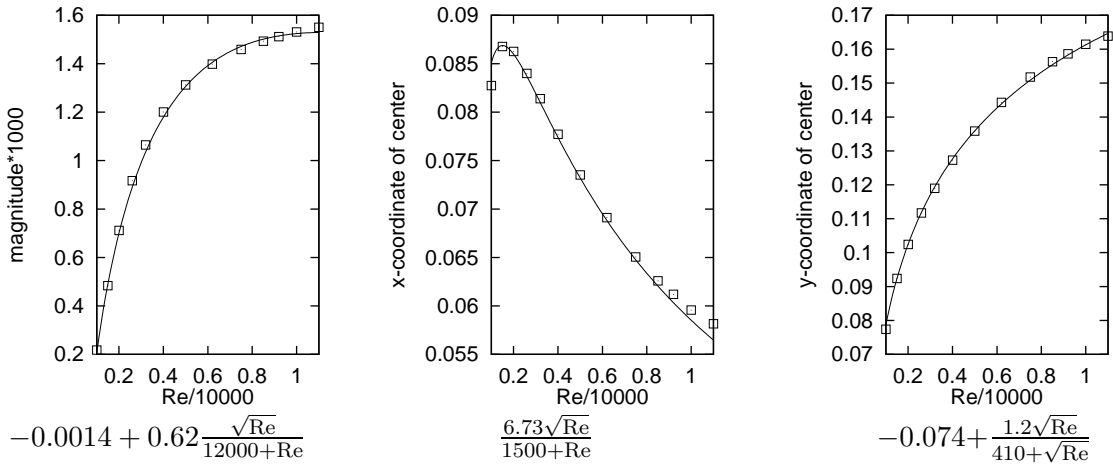
Рис. 9. Vortex characteristics as functions of Re : \diamond —[18]; \square — present results from Richardson extrapolation with 256 and 512 grids; $+$ present results from Richardson extrapolation with 128 and 256 grids; — or - - - — empirical best fit.

steady-state flow is already unstable and can never be realized in the nature or in the true-time algorithms. This leaves open the question of whether a steady-state solution is a valid physical option for the lid-driven cavity flow at larger Reynolds numbers.

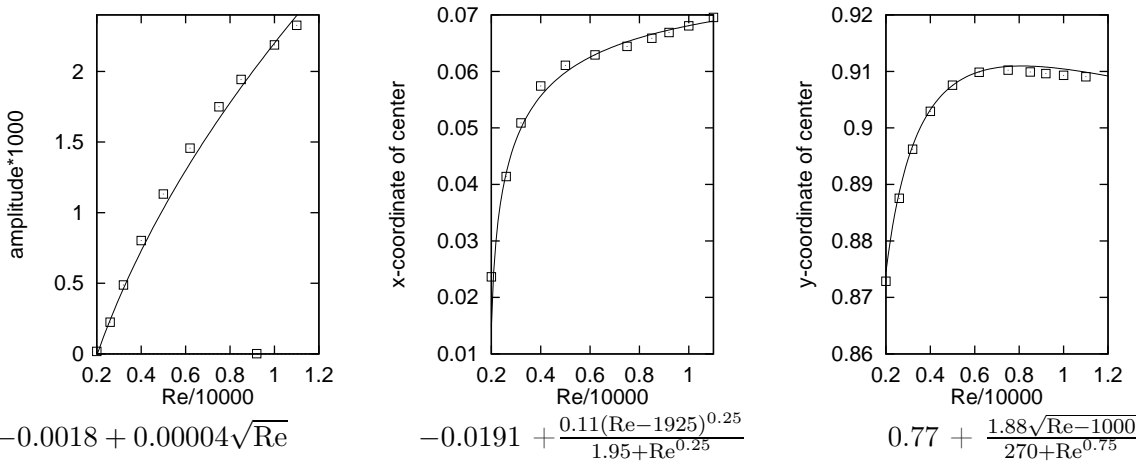
The only information to be obtained through a false-transient algorithm is the shape of the steady-state streaming when it exists. Even this requires extensive computations because of the prohibitive amount of computational time. We will treat this problem in a separate work after some optimizations are introduced in the code. The accent of the present work is on the vectorial splitting rather than on the exhaustive treatment of the cavity flow.

7. Conclusions

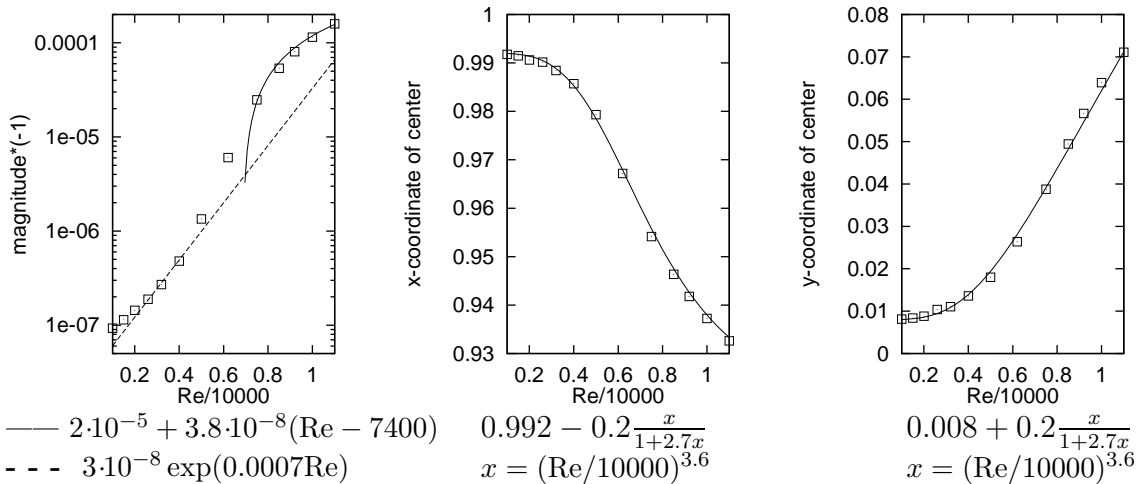
The steady flow of incompressible viscous liquid in rectangular enclosures is considered. The Navier—Stokes equations and the incompressibility constraint are rendered to an elliptic system containing a Poisson-type equation for the pressure *in lieu* of the continuity equation. Unlike the classical Poisson equation for pressure, the equation derived here comprises also the



c Secondary vortex in the bottom left corner;



d Secondary vortex in the top left corner;



e Tertiary vortex in the bottom right corner.

Рис. 9. (Continuation).

original continuity equation as an additional term. This proves essential for the stability of the false-transients method and for the application of operator splitting. We have shown that the new system is equivalent to the original N-S provided that the continuity condition is imposed

as an additional boundary condition and *no* boundary conditions for the pressure function are specified.

A novel and computationally efficient *vectorial* implicit operator-splitting method for solving the evolution system is developed. The vectorial splitting is essential in preserving the coupling between the velocity and pressure at each fractional time step. Thus the boundary conditions are resolved in fully implicit fashion avoiding the need to impose the Thom's condition. The nonlinear terms are approximated by conservative central differences. Although devoid of artificial ("scheme") viscosity our scheme is shown to be stable for reasonable time increments of order $\tau = 0.05$ even for very high Reynolds numbers.

The advantages of the new difference scheme can be summarized as follows:

- The scheme is fully implicit with regard to the boundary conditions. It is strongly implicit as far as the nonlinear terms in the momentum equations are concerned in the sense that the derivatives are taken on the new time stage while the velocity components play the role of "frozen coefficients" taken from the previous time step.
- The artificial ("scheme") viscosity is eliminated by means of conservative symmetric approximation of the nonlinear terms. Hence the results for high Reynolds numbers do not depend on the so-called "cell" Reynolds number hRe as the upwind and TVD schemes do.
- The operator-splitting of the linear elliptic operators reduces by orders of magnitude the needed computational time per time step in comparison with the implicit schemes employing inversion of the non-split operators.
- The scheme employs primitive variables and its generalization to 3D is straightforward.

As a featuring example the lid-driven viscous incompressible flow in a rectangular cavity is treated by the new scheme. The mandatory numerical experiments for consistency and stability of the scheme are performed involving different grids: 16×16 ; 32×32 ; 64×64 ; 128×128 ; 256×256 and 512×512 cells. The consistency and convergence of the scheme is shown analytically and verified numerically via mandatory tests with different resolutions and time increments. Calculations on the finest grid are found to converge in time for Reynolds number up to $Re = 11000$. Results for the flow pattern are in very good quantitative agreement with the known results from the literature in this range of Reynolds number. More subtle flow characteristics, such as magnitudes and position of the primary, secondary, and tertiary vortices, are also calculated. Their dependence on Reynolds number is much smoother in the present work in comparison with the available data from the literature.

For the particular problem under consideration, new information is obtained in the present work for high Reynolds numbers which may serve as a basis of further in-depth asymptotic study of the physical properties of the lid-driven flow in a rectangular cavity. The information is organized as empirical best-fit correlations.

References

- [1] ABDALLAH S. Numerical solutions for the pressure Poisson equation with Neumann boundary condition using a non-staggered grid. Pt I // J. Comp. Phys. 1987. Vol. 70. P. 182–192.

- [2] ABDALLAH S. Numerical solutions for the incompressible Navier—Stokes equations in primitive variables using a non-staggered grid. Pt II // *J. Comp. Phys.* 1987. Vol. 70. P. 193–202.
- [3] ARAKAWA A. Computational design for long-term numerical integration of the equations of fluid motion: Two-dimensional incompressible flow. Pt I // *J. Comp. Phys.* 1966. Vol. 1. P. 119–143.
- [4] BENJAMIN A. S., DENNY V. E. On the convergence of numerical solutions for the 2-D flows in a cavity at large Re // *J. Comp. Phys.* 1979. Vol. 33. P. 340–358.
- [5] BRUNEAU C.-H., JOURON C. An efficient scheme for solving steady incompressible Navier—Stokes equations // *J. Comp. Phys.* 1990. Vol. 89. P. 389–413.
- [6] BURGGRAF O. Analytical and numerical studies of the structure of steady separated flows // *J. Fluid Mech.* 1966. Vol. 24. P. 113–151.
- [7] CHRISTOV C. I. Method of variational imbedding for elliptic incorrect problems // *Comp. Rend. Acad. Bulg. Sci.* 1996. Vol. 39, No. 12. P. 23–26.
- [8] CHRISTOV C. I. Gaussian elimination with pivoting for multidagonal systems // Internal Report. Vol. 4. Univ. of Reading, 1994.
- [9] CHRISTOV C. I., MARINOVA R. S. Numerical investigation of high Re stationary viscous flow around circular cylinder as inverse problem // *Bulg. J. Meteorology and Hydrology.* 1994. Vol. 5, No. 3–4. P. 105–118.
- [10] CHRISTOV C. I., PONTES J., WALGRAEF D., VELARDE M. G. Implicit time splitting for fourth-order parabolic equations // *Comp. Methods in Appl. Mech. Engn.* 1997. Vol. 148. P. 209–224.
- [11] CHRISTOV C. I., RIDHA A. Splitting scheme for iterative solution of bi-harmonic equation. Application to 2D Navier—Stokes problems // *Advances in Numer. Methods and Appl.* Singapore: World Sci., 1994. P. 341–352.
- [12] CHRISTOV C. I., RIDHA A. Splitting scheme for the stream-function formulation of 2D unsteady Navier—Stokes equations // *C. R. Acad. Sci. Paris.* 1995. Vol. 320. II b. P. 441–446.
- [13] CHRISTOV C. I., RIDHA A. Splitting scheme for stream-function formulation of Navier—Stokes equations. Pt I. Stationary case. 1999 (to be submitted).
- [14] CHURBANOV A. G., PAVLOV A. N., VABISHCHEVICH P. N. Operator-splitting methods for the incompressible Navier—Stokes equations on non-staggered grids. Pt 1: First order schemes // *Intern. J. Num. Meth. Fluids.* 1995. Vol. 21. P. 617–640.
- [15] DE VAHL DAVIS G., MALLISON G. D. An evaluation of upwind and central difference approximations by a study of recirculating flow // *Comput. Fluids.* 1976. Vol. 4. P. 29–43.
- [16] DOUGLAS J. On the Numerical integration of $\partial^2 u / \partial x^2 + \partial^2 u / \partial y^2$ by implicit methods // *SIAM J.* 1955. Vol. 3. P. 42–65.

- [17] FORNBERG B. A numerical study of steady viscous flow past a circular cylinder // *J. Fluid Mech.* 1980. Vol. 98. P. 819–835.
- [18] GHIA U., GHIA K. N., SHIN C. N. High-Re solutions for incompressible flow using the Navier–Stokes equation and a multigrid method // *J. Comp. Phys.* 1982. Vol. 48. P. 387–411.
- [19] GOYON O. High-Reynolds number solutions of Navier–Stokes equation using incremental unknowns // *J. Comput. Methods Appl. Mech. Engrg.* 1996. Vol. 130. P. 319–355.
- [20] GRESHO P. M. Incompressible fluid dynamics: Some fundamental formulation issues // *Ann. Rev. Fluid Mech.* 1991. Vol. 23. P. 413–453.
- [21] GRESHO P. M., CHAN S. T. On the theory of semi-implicit projection methods for viscous incompressible flow and its implementation via a finite element method that also introduces a nearly consistent mass matrix. Pt 2: Implementation // *Intern. J. Numer. Methods Fluids.* 1990. Vol. 11. P. 621–659.
- [22] GRESHO P. M., SANI R. L. On pressure boundary conditions for the incompressible Navier–Stokes equations // *Intern. J. Numer. Methods Fluids.* 1987. Vol. 7. P. 1111–1145.
- [23] GUPTA M. M. High accuracy solutions of incompressible Navier–Stokes equations // *J. Comp. Phys.* 1991. Vol. 93. P. 343–359.
- [24] HENSHAW A. D. A fourth-order accurate method for the incompressible Navier–Stokes equations on overlapping grids // *J. Comp. Phys.* 1994. Vol. 113. P. 13–35.
- [25] HENSHAW A. D., KREISS H.-O., REYNA L. G. M. A fourth-order accurate difference approximation for the incompressible Navier–Stokes equations // *Comput. Fluids.* 1994. Vol. 23. P. 575–593.
- [26] ILIEV O. P., MAKAROV M. M. A block-matrix iterative numerical method for coupled solving 2D Navier–Stokes equations // *J. Comp. Phys.* 1995. Vol. 121. P. 324–330.
- [27] KARNAIDAKIS G., ISRAELI M., ORSZAG S. A. High-order splitting methods for the incompressible Navier–Stokes equations // *J. Comp. Phys.* 1991. Vol. 97. P. 414–443.
- [28] KIM J., MOIN P. Application of fractional-step method to incompressible Navier–Stokes equations // *J. Comp. Phys.* 1985. Vol. 59. P. 308–323.
- [29] LIAO S. J., ZHU J. M. A short note on high-order streamfunction-vorticity formulation of 2D steady state Navier–Stokes equations // *Intern. J. Num. Meth. Fluids.* 1996. Vol. 22. P. 1–9.
- [30] MALLISON G. D., DE VAHL DAVIS G. The method of false transients for the solution of coupled elliptic equations // *J. Comp. Phys.* 1973. Vol. 12. P. 435–461.
- [31] MARCHUK G. I. *Methods of Numerical Mathematics.* Berlin: Springer-Verlag, 1982.
- [32] QUARTAPELLE L. Vorticity conditioning in the computation of two-dimensional viscous flows // *J. Comp. Phys.* 1981. Vol. 40. P. 453–477.

- [33] RAMASWAMY B. Theory and implementation of a semi-implicit finite-element method for viscous incompressible flow // *Comp. Fluids*. 1993. Vol. 22. P. 725–747.
- [34] ROSENFELD M., KWAK D., VINOKUR M. A fractional step solution method for the unsteady incompressible Navier — Stokes equations in generalized coordinate system // *J. Comp. Phys*. 1991. Vol. 94. P. 102–137.
- [35] RUBIN S. G., KHOSLA P. K. Navier — Stokes calculations with a coupled strongly implicit method-I // *Comput. Fluids*. 1981. Vol. 9. P. 163–180.
- [36] SCHREIBER R., KELLER H. B. Driven cavity flows by efficient numerical techniques // *J. Comp. Phys*. 1983. Vol. 49. P. 310–333.
- [37] SHEN J. Hopf bifurcation of the unsteady regularized driven cavity flow // *J. Comp. Phys*. 1991. Vol. 95. P. 228–245.
- [38] SMAGULOV SH., CHRISTOV C.I. Iterationless numerical implementation of the boundary conditions in vorticity-stream function formulation of Navier — Stokes equations. Preprint 20. *Inst. Theor. Appl. Mech., Russian Acad. Sci., Novosibirsk*, 1980.
- [39] SOH W. Y. Time-marching solution of incompressible Navier — Stokes equations for internal flow // *J. Comp. Phys*. 1987. Vol. 70. P. 232–252.
- [40] STRIKWERDA J. C. *Finite difference schemes for partial differential equations*. Chapman & Hall.
- [41] STRIKWERDA J. C. Finite-difference methods for the Stokes and Navier — Stokes equations // *SIAM J. Sci. Stat. Comp*. 1984. Vol. 5. P. 56–68.
- [42] TEMAM R. *Navier — Stokes Equations*. Amsterdam: North-Holland, 1977.
- [43] THOMPSON M. C., FERZIGER J. H. An adaptive multigrid technique for the incompressible Navier — Stokes equations // *J. Comp. Phys*. 1989. Vol. 82. P. 94–121.
- [44] TUREK S. Tools for simulating non-stationary incompressible flow via discretely divergence-free finite element models // *Intern. J. Num. Meth. Fluids*. 1994. Vol. 18. P. 71–105.
- [45] VABISHCHEVICH P. N. Implicit finite-difference schemes for the nonstationary Navier — Stokes equations with the stream function and vorticity as variables // *Differential Equations*. 1984. Vol. 20. P. 820–827.
- [46] VANKA S. P. Block-implicit multigrid solution of Navier — Stokes equations in primitive variables // *J. Comp. Phys*. 1986. Vol. 65. P. 138–158.
- [47] WRIGHT J. A., SHYY W. A pressure-based composite grid method for the Navier — Stokes equations // *J. Comp. Phys*. 1993. Vol. 107. P. 225–238.
- [48] YANENKO N. N. *Method of Fractional Steps*. Berlin: SpringerVerlag, 1971.